

Contents lists available at ScienceDirect

Fundamental Research

journal homepage: <http://www.keaipublishing.com/en/journals/fundamental-research/>

Article

Twisted lattice nanocavity with theoretical quality factor exceeding 200 billion

Ren-Min Ma^{a,b,c,d,*}, Hong-Yi Luan^a, Zi-Wei Zhao^a, Wen-Zhi Mao^a, Shao-Lei Wang^a, Yun-Hao Ouyang^a, Zeng-Kai Shao^a^a State Key Laboratory for Mesoscopic Physics and Frontiers Science Center for Nano-Optoelectronics, School of Physics, Peking University, Beijing 100871, China^b Collaborative Innovation Center of Quantum Matter, Beijing 100871, China^c Peking University Yangtze Delta Institute of Optoelectronics, Nantong 226010, Jiangsu, China^d National Biomedical Imaging Center, Peking University, Beijing 100871, China

ARTICLE INFO

Article history:

Received 6 October 2022

Received in revised form 28 October 2022

Accepted 7 November 2022

Available online 18 November 2022

Keywords:

Nanocavities
Twisted lattice
Quality factor
Mode volume
Flatband
Mode coupling

ABSTRACT

Simultaneous localization of light to extreme spatial and spectral scales is of high importance for testing fundamental physics and various applications. However, there is a longstanding trade-off between localizing a light field in space and in frequency. Here we discover a new class of twisted lattice nanocavities based on mode locking in momentum space. The twisted lattice nanocavity hosts a strongly localized light field in a $0.048 \lambda^3$ mode volume with a quality factor exceeding 2.9×10^{11} ($\sim 250 \mu\text{s}$ photon lifetime), which presents a record high figure of merit of light localization among all reported optical cavities. Based on the discovery, we have demonstrated silicon-based twisted lattice nanocavities with quality factor over 1 million. Our result provides a powerful platform to study light-matter interaction in extreme conditions for tests of fundamental physics and applications in nanolasing, ultrasensing, nonlinear optics, optomechanics and quantum-optical devices.

1. Introduction

From Planck's law on blackbody radiation to Fermi's golden rule and Purcell effect, the notion that a radiation process depends not only on the intrinsic properties of an emitter but also on its surrounding environment lays the foundation for the understanding and developing of light-matter interaction related fields [1–6]. However, light-matter interaction is in general a weak process due to the mismatched wavelength of photons and electrons. In decades, artificial microstructures represented by metamaterials have been developed to enlarge and manipulate photon density of states to enhance light-matter interaction [3,7–19]. In terms of that, the ratio of quality factor over mode volume (Q/V) represents a key figure of merit, because it characterizes how strongly a light field can be confined on both spatial and spectral scales.

Because of the applicable finite potential well in photonics, there is a longstanding trade-off between confining a light field in space and in frequency. Localization mechanisms including total internal reflection [20–28], photonic bandgap [29–38], plasmonic resonance [39–44] and bound states in the continuum (BICs) [45–49] have been developed for decades to design optical cavities with high Q/V for high-performance

lasers, nonlinear optics, optomechanics and quantum-optical devices and so on. However, the trade-off limits the highest figure of merit of Q/V available. Dielectric whispering-gallery-mode microcavities based on total internal reflection can achieve quality factor over a billion, but with a mode volume orders of magnitude larger than λ^3 (λ : free space wavelength) [20,22,28]. A plasmonic nanocavity employing atomistic protrusion on a host nanoparticle can achieve a mode volume as small as 1 nm^3 , but with a limited quality factor around 10 [44]. Photonic crystal nanocavities can achieve near the diffraction-limited mode volume, but to achieve high quality factor needs complicated design for a full band gap and judiciously tuned wavefunction [29–38]. For instance, deep learning has been employed to optimize the quality factor of photonic crystal nanocavities, where a Q factor of 1.58×10^9 was obtained after optimizing the positions of 50 holes over $\sim 10^6$ iterations [36]. BICs can be used to localize a light field in one dimension with infinite quality factor but at the cost of a fully delocalized field in the other two dimensions. Quasi-BIC cavities with finite lateral size have been constructed to achieve high Q/V . The highest realized Q/V is about $2.5 \times 10^6 \lambda^{-3}$, where the quality factor and mode volume are 1.09×10^6 and $0.43 \lambda^3$, respectively [49].

* Corresponding author.

E-mail address: renminma@pku.edu.cn (R.-M. Ma).<https://doi.org/10.1016/j.fmre.2022.11.004>2667-3258/© 2022 The Authors. Publishing Services by Elsevier B.V. on behalf of KeAi Communications Co. Ltd. This is an open access article under the CC BY-NC-ND license (<http://creativecommons.org/licenses/by-nc-nd/4.0/>)

Recently, flatband induced wavefunction localization in moiré superlattices has drawn great attention in electronic [50–52], photonic [53–58] and phononic systems [59–64]. Compared to conventional laser cavities where discontinuity of material property or disorder is required of light field localization, flatband induced field localization can be realized in periodic moiré superlattices. However, notwithstanding the fast development of work on photonic moiré cavities, the highest Q/V achieved is yet many orders of magnitude lower than those of conventional laser cavities. Further, flatbands correspond to periodic structures, which naturally require a very large footprint.

Here, we propose and demonstrate a field localization mechanism of mode locking in momentum space in an artificial twisted lattice system, and report a new class of twisted lattice nanocavities with Q/V over $6 \times 10^{12} \lambda^{-3}$, which is more than one order of magnitude higher than those of all reported optical cavities. The twisted lattice nanocavities are constructed by truncating a finite part of two twisted photonic crystals introduced into a single layered dielectric membrane. We find that the twisted lattice supplies an adiabatic potential for strongly localizing a light field at the deep subwavelength scale with an ever increasing quality factor with the decreasing of the twisted angle. In stark contrast to the well-studied flatband induced mode localization, twisted lattice nanocavities have much smaller footprints and are free from periodicity requirement - the twisted angle between the two sets of lattices can be arbitrary, which greatly simplifies the fabrication procedure and provides a powerful platform for studying light-matter interaction in extreme conditions and applications. To demonstrate the applications of twisted lattice nanocavities, we have constructed silicon-based twisted lattice nanocavities based on silicon on insulator (SOI) substrates, where the experimentally demonstrated quality factor is over 1 million.

2. Methods

2.1. Full-wave simulation

In the simulation and experiment, we use two sets of triangular lattices of nanoholes in the same membrane with a twisted angle to construct twisted lattice nanocavities. Each of triangular lattice of nanoholes defines a photonic graphene lattice in the membrane [55]. Eigenmodes of twisted lattice nanocavities based on silicon membrane are obtained by three-dimensional full wave simulations via finite-element method based on the commercial software of COMSOL Multiphysics. From the eigenmodes, field distributions, quality factors and

mode volumes of twisted lattice nanocavities can be obtained. The mode volume is calculated by $V = \frac{\int \epsilon(\mathbf{r})|E(\mathbf{r})|^2 d^3r}{\max[\epsilon(\mathbf{r})|E(\mathbf{r})|^2]}$, where $\epsilon(\mathbf{r})$ is position dependent permittivity of the simulated structure. The quality factor is calculated by $Q = (Re[f])/(2Im[f])$, where $Re[f]$ and $Im[f]$ are the real and imaginary part of the eigenfrequency of a simulated cavity eigenmode.

2.2. Fabrication of silicon based twisted lattice nanocavities

Silicon on insulator (SOI) substrates are used to fabricate twisted lattice nanocavities. Electron beam lithography is used to define the device pattern where two sets of nanoholes with a twisted angle are drawn together to the E-beam resist. Inductively coupled plasma etching is processed to etch holes in the top silicon layer. Buffered hydrofluoric acid is used to etch away the buried oxide layer to form a suspended membrane for the cavity test (Supplementary Fig. 5). In the two sets of twisted photonic graphene lattices of the nanocavity at 4.41° , the diameter of the nanoholes is 220 nm, and the lattice constant is 500 nm. In the two sets of twisted photonic graphene lattices of the nanocavity at 0.596° , the diameter of the nanoholes is 210 nm, and the lattice constant is 460 nm. The thickness of the silicon membrane is 220 nm.

2.3. Optical characterization of silicon based twisted lattice nanocavities

A tunable continuous wave laser is used to excite the eigenmodes of the twisted lattice nanocavities. The laser beam is first sent through a chopper for lock-in detection. The chopped beam is sent through a polarizer and then a $100\times$ microscope objective with a numerical aperture of 0.85 to be focused on the cavity. The scattering field of the excitation laser beam is collected by the same objective and sent to another polarizer and then infrared photodetector connected to a lock-in amplifier. The two polarizers are set orthogonally to filter the directly reflected light to enhance the signal-to-noise ratio. The optical setup is shown in Supplementary Fig. 6.

3. Construction of twisted lattice nanocavities

The twisted lattice nanocavities are constructed by truncating two sets of photonic crystals with a twist (Fig. 1). In the structure, two sets of photonic graphene lattices with a twist are introduced to the same dielectric membrane [55] to simplify the fabrication procedure and to enhance the coupling strength between Bloch modes of the two sets of the photonic crystals. For those twisted angles at which periodic moiré

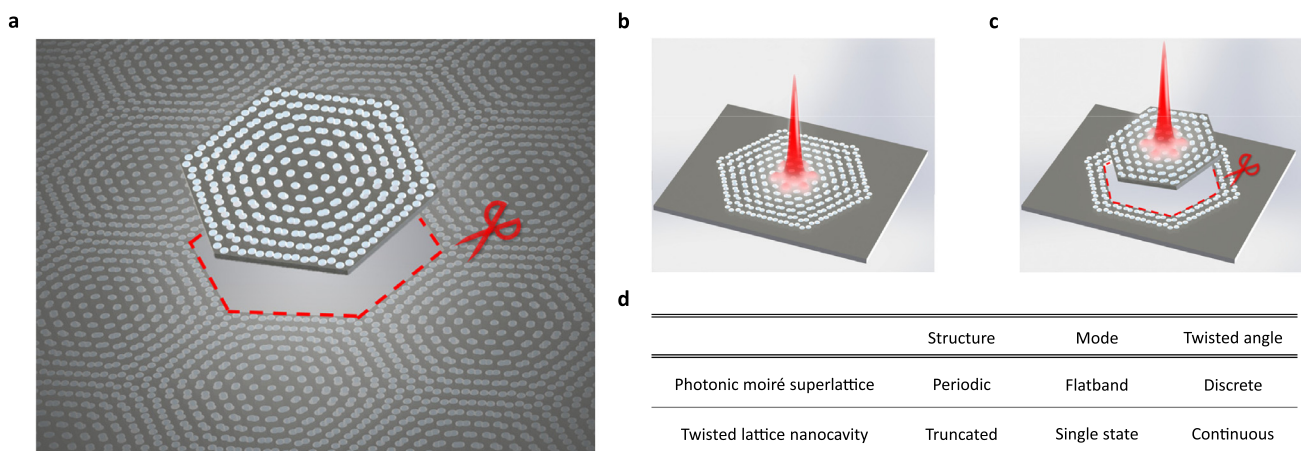


Fig. 1. Construction of twisted lattice nanocavities. (a) A twisted lattice nanocavity is constructed by truncating two sets of photonic crystals with a twist. (b) Schematic of a twisted lattice nanocavity with the localized light field in the center. (c) The twisted lattice nanocavity depicted in (b) can be further truncated to have an even smaller footprint. (d) Comparison between photonic moiré superlattices and twisted lattice nanocavities.

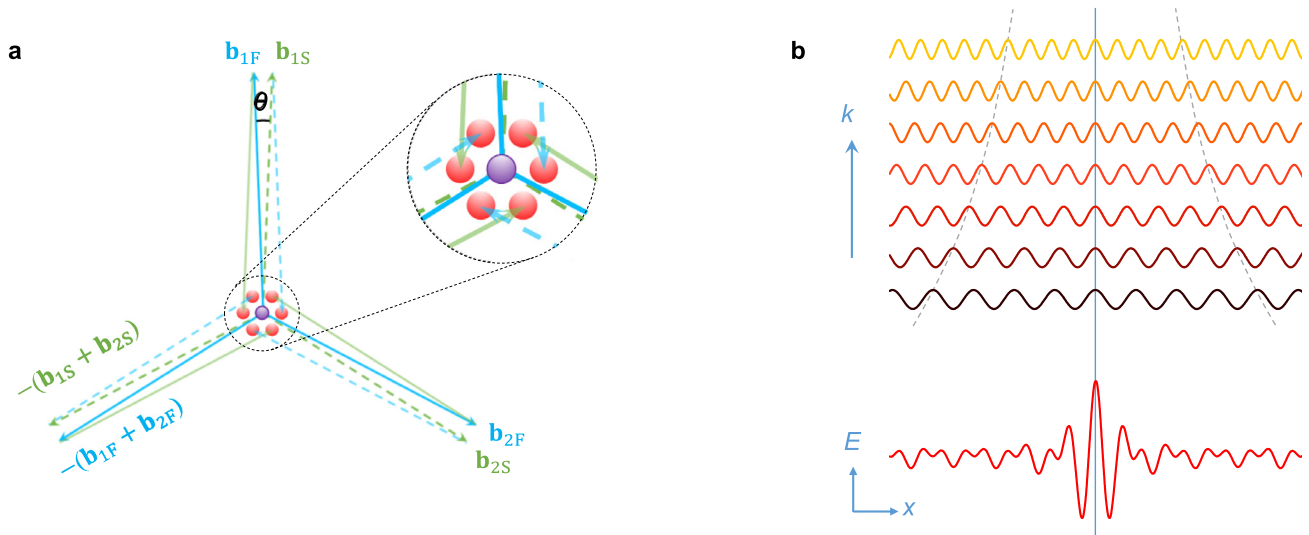


Fig. 2. Field localization of twisted lattice nanocavities by mode locking in momentum space. (a) Schematic of Bloch modes coupling induced by reciprocal lattice vectors of the two sets of twisted photonic crystals, where the Bloch mode indicated by purple dot is coupled to six other Bloch modes indicated by red dots via $\pm(G_F - G_S)$. G_F : reciprocal lattice vectors of the first set of photonic crystal. G_S : reciprocal lattice vectors of the second set of photonic crystal. Three blue arrows indicate G_F of b_{1F} , b_{2F} and $-(b_{1F} + b_{2F})$, and three dashed green arrows indicate G_S of b_{1S} , b_{2S} and $-(b_{1S} + b_{2S})$, where b_{1F} , b_{2F} are two basis vectors of G_F , and b_{1S} , b_{2S} are two basis vectors of G_S (Supplementary Note 1). (b) Schematic of the coupling induced mode locking in momentum space, which results in Bloch modes localization in real space. E , x , and k are electric field, position and wavevector respectively.

superlattices can be constructed, we use a single moiré unit cell to construct the nanocavities (Supplementary Fig. 1a). For those twisted angles at which periodic moiré superlattices cannot be constructed, we use a quasi-single moiré unit cell (Supplementary Fig. 1b). For the constructed nanocavities, a smaller twisted angle corresponds to a larger physical cavity size (Supplementary Fig. 2). Because the desired mode is tightly localized in the center of the nanocavity, we can use a further truncated cavity with an even smaller physical size (Fig. 1c). Fig. 1d provides a direct comparison between photonic moiré superlattices and twisted lattice nanocavities, where key features of these two structures are listed.

4. Strong field localization based on mode locking in momentum space

The strong field localization in twisted lattice nanocavities originates from Bloch modes coupling induced by reciprocal lattice vectors of the two sets of twisted photonic crystals (Fig. 2a, Supplementary Note 1). In a single set of photonic crystal, Bloch modes are delocalized waves spanning the whole area of the photonic crystal, and only those modes differing in a reciprocal lattice vector (denoted as G_F) can couple to each other. After introducing the second set of photonic crystal, a Bloch mode can couple to other Bloch modes when their momenta differ in $\pm(G_F - G_S)$, where G_S is denoted as reciprocal lattice vectors of the second set of photonic crystal. The coupling induces mode locking in momentum space, which results in the localization of originally delocalized Bloch modes in real space (Fig. 2b).

We can see that the localization mechanism of twisted lattice nanocavities does not put any constraints on the twisted angle – one can continuously change the twisted angle to obtain a localized light field. As a comparison, to form a moiré superlattice, the twisting has to be made in a certain set of discrete angles, where $\pm(G_F - G_S)$ becomes moiré reciprocal lattice vectors corresponding to moiré periodicity.

A photonic graphene lattice can be viewed as a triangular lattice consisting of hexagonal unit cells with 6 sites. We use 2 degenerate dipole modes of $|p_x\rangle$ and $|p_y\rangle$ and 2 degenerate quadrupole modes of $|d_{x^2-y^2}\rangle$ and $|d_{xy}\rangle$ of one unit cell of 6 sites as Wannier functions to construct Bloch modes in a single set of photonic graphene lattice (Supplementary Note 1). Due to the interlayer coupling by $\pm(G_F - G_S)$, these four modes

will become localized modes in the center of twisted lattice nanocavities. Throughout the work, we focus on the localized dipole modes with smaller mode volumes in twisted lattice nanocavities.

5. Ultrahigh figure of merit of quality factor over mode volume

Fig. 3a shows field distribution patterns of a twisted lattice nanocavity at 4.41° obtained by three-dimensional full wave simulation (Methods). We can see that the dipole mode is strongly localized in the center of the nanocavity in all three dimensions. Fig. 3b and the blue curve of Fig. 3c show the mode profile and the mode volume of the dipole mode at varied twisted angles where all other parameters of the two sets of graphene photonic crystals are fixed. Clearly, the mode volume of the localized dipole mode almost does not change with the twisted angle.

Remarkably, the quality factor of the localized dipole mode continuously increases with the decreasing of the twisted angle (red curve of Fig. 3c). As shown in figure, the scaling of quality factor over twisted angle has a kink around 4.41° , which originates from the transition from the in-plane scattering loss dominant region to the out-of-plane scattering loss dominant region (Fig. 3d). A larger angle gives a smaller cavity size, which results in a comparably stronger field at cavity boundaries that can be coupled to free propagating modes of the membrane, leading to a larger in-plane scattering loss. At smaller twisted angles, cavity size becomes larger, therefore such in-plane scattering loss substantially decreases. Around the twisted angle of 4.41° , out-of-plane scattering loss becomes dominant.

Interestingly, a smaller twisted angle will also suppress out-of-plane scattering loss to free space. With the decreasing of the twisted angle, the arrangement of nanoholes from the center to the boundaries of a cavity changes more slowly (SEM images in Fig. 5b and Fig. 6b). However, the intensity distribution of the wavefunction of the localized dipole modes has almost no change – it keeps being tightly localized in the center of the nanocavities with the decreased angle. Therefore, at a smaller angle, the wavefunction of a localized dipole mode experiences a more effective adiabatic change in the arrangement of nanoholes towards cavity boundaries, leading to a lower scattering loss to free space and a higher vertical Q. In the out-of-plane scattering loss dominant region, we can use a truncated cavity with a relatively small physical size for easier

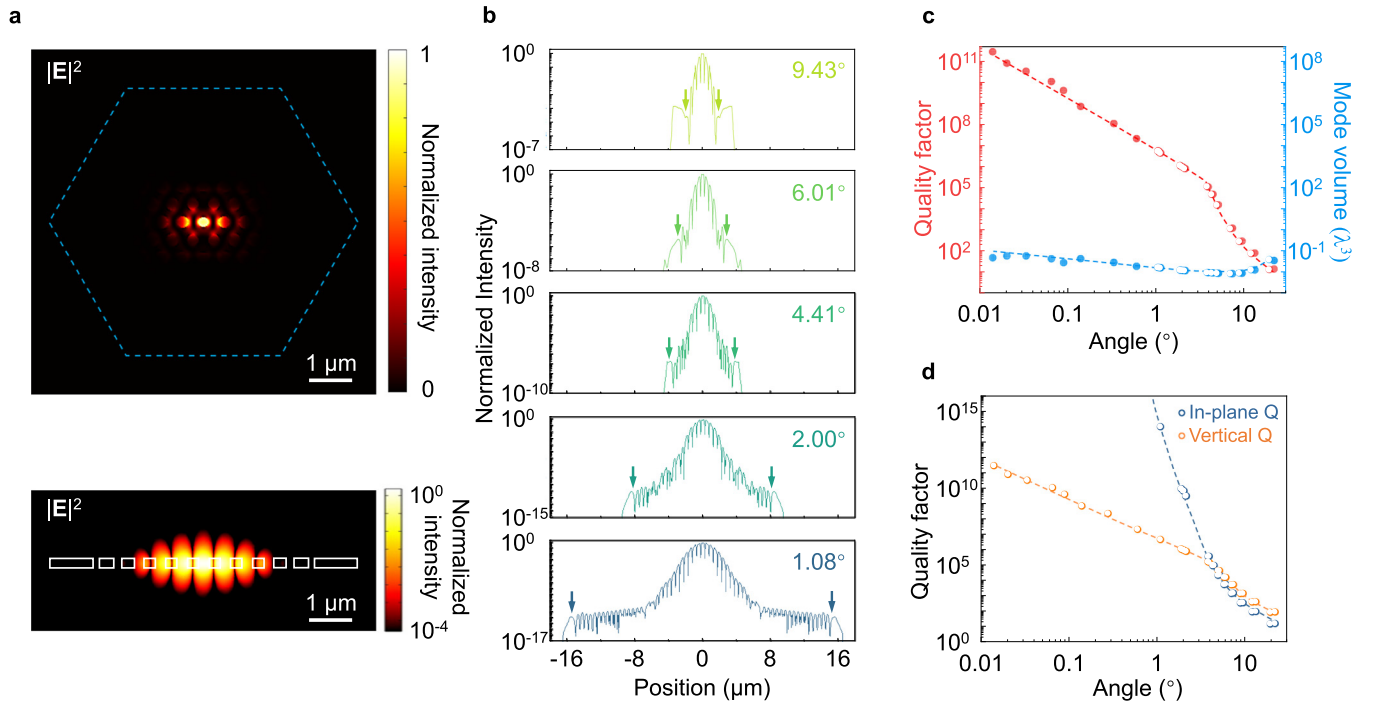


Fig. 3. Ultrahigh figure of merit of field localization of twisted lattice nanocavities. (a) Electric field intensity $|E|^2$ distribution of the localized mode induced by mode locking in momentum space. Blue dashed hexagon indicates the cavity boundary. Bottom: Electric field intensity distribution in log scale in a cross-section of the cavity. White boxes: contour of the cavity structure. (b) Intensity distributions of the localized dipole modes in log scale at five twisted angles. The mode keeps being strongly localized with the decreasing of the twisted angle. Arrows indicate cavity boundaries. (c) The scaling laws of quality factor (Q) and mode volume (V) vs. twisted angle obtained by three-dimensional full wave simulation where all the parameters of the two sets of graphene photonic crystals are fixed. Dots and circles represent angles that periodic moiré superlattices can and cannot be constructed respectively. (d) Scaling laws of in-plane and vertical quality factor of twisted lattice nanocavities. Dots: data. Lines: fitting.

fabrication while maintaining a high quality factor (Supplementary Fig. 4).

The quality factor reaches 2.9×10^{11} at 0.0138° , with a corresponding mode volume of $0.048 \lambda^3$, which results in a Q/V of $\sim 6 \times 10^{12} \lambda^{-3}$, which is more than one order of magnitude higher than those of all reported optical cavities to our knowledge (Fig. 4). The highest Q/V presented in Fig. 4 is only limited by our computing power in three-dimensional full wave simulation. The twisted lattice nanocavity can achieve ever increasing Q/V by just simply making the twisted angle smaller, which provides a powerful platform to pursue ever increasing field enhancement in a nanocavity.

6. Silicon based twisted lattice nanocavities

Experimentally, we fabricate twisted lattice nanocavities in silicon membrane from SOI substrates (Methods and Supplementary Fig. 5). Fig. 5a-b show the scanning electron microscopy (SEM) images of a twisted lattice nanocavity at the twisted angle of 4.41° . The red and yellow circles in Fig. 5b indicate two lines of nanoholes from the twisted two graphene lattices. A tunable continuous wave laser is used to excite the localized dipole mode in the fabricated nanocavities (Methods and Supplementary Fig. 6). The cavity holds a localized mode in the center area that can be excited under the resonance condition. Fig. 5c-d show the experimentally excited and full wave simulated patterns of the localized dipole mode in the cavity, which match well with each other (Fig. 5e). The resonance wavelength and linewidth of the mode are 1558.67 nm and 89 pm, respectively (Fig. 5f), which yields a quality factor of $\sim 1.75 \times 10^4$.

The quality factor of the mode increases with the decreasing angle because of the more adiabatic potential as discussed above. We further fabricate a twisted lattice nanocavity at a smaller twisted angle

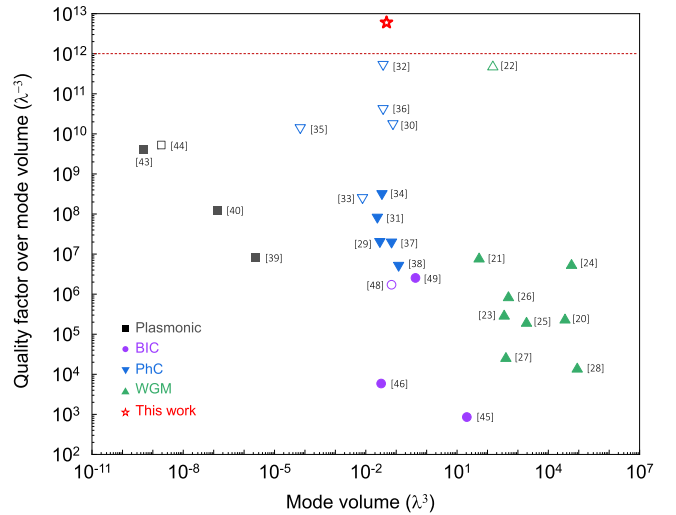


Fig. 4. Comparison of quality factor over mode volume (Q/V) with other representative optical cavities. Q/V versus V of twisted nanocavity, whispering-gallery-mode (WGM) microcavities, photonic crystal (PhC) nanocavities, plasmonic nanocavities, bound-state-in-the-continuum (BIC) microcavities. Hollow: quality factor obtained by simulation. Solid: quality factor obtained by experiment.

of 0.596° . Fig. 6 shows the SEM images and the optical characterization results. Due to the small twisted angle, the pattern of the nanoholes in the center area of the cavity is close to that of a single set of photonic graphene lattice (Fig. 6a-b). Fig. 6c-d show the experimentally excited and full wave simulated patterns of the localized dipole mode in the cavity, which match well with each other (Fig. 6e). The resonance

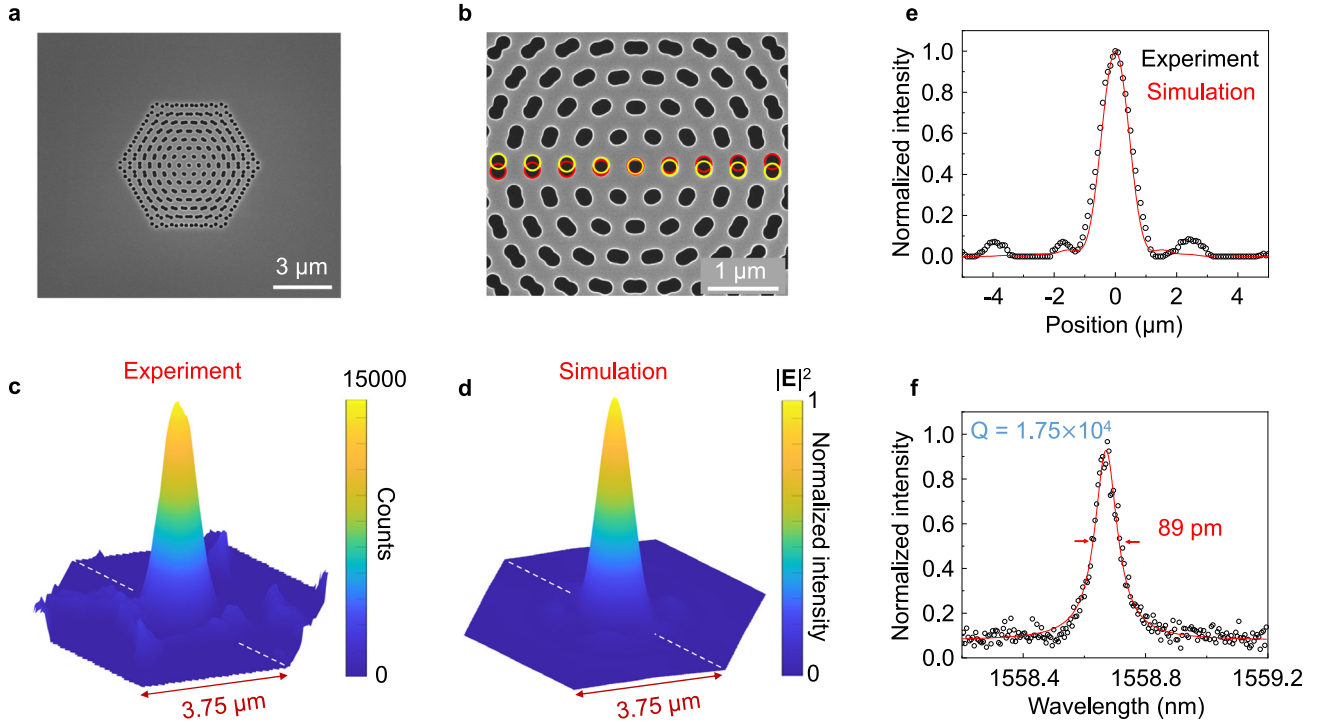


Fig. 5. Silicon based twisted lattice nanocavity at the twisted angle of 4.41°. (a) SEM image of the silicon based twisted lattice nanocavity at the twisted angle of 4.41°. (b) Enlarged SEM image of the cavity shown in (a). Red and yellow circles guide the eye to the twisting of the lattices. (c-d) Experimentally excited (c) and full wave simulated (d) localized dipole mode of the cavity. (e) Intensity distributions of the localized mode along the white dashed lines in (c) and (d). (f) Experimentally measured scattering spectrum of the nanocavity. The resonance wavelength and linewidth of the mode are 1558.67 nm and 89 pm respectively, which gives a quality factor $\sim 1.75 \times 10^4$.

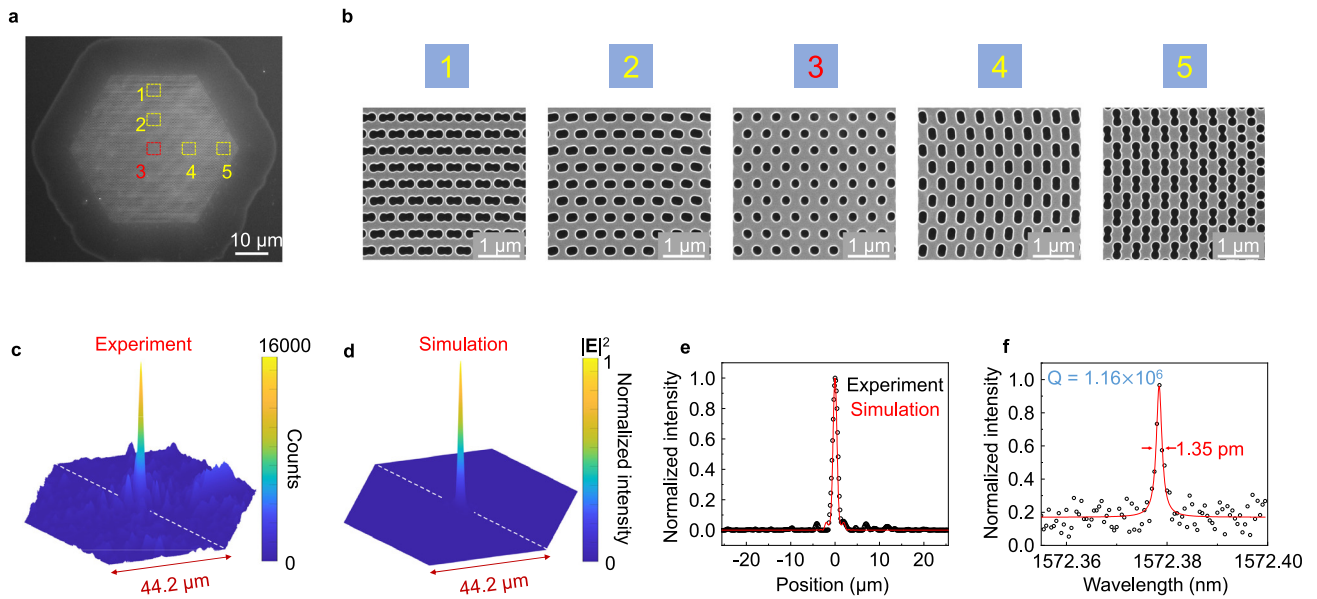


Fig. 6. Silicon based twisted lattice nanocavity at the twisted angle of 0.596°. (a) SEM image of the silicon based twisted lattice nanocavity at the twisted angle of 0.596°. (b) Enlarged SEM images of the areas indicated in (a). (c-d) Experimentally excited (c) and full wave simulated (d) localized dipole mode of the cavity. (e) Intensity distributions of the localized mode along the white dashed lines in (c) and (d). (f) Experimentally measured scattering spectrum of the nanocavity. The resonance wavelength and linewidth of the mode are 1,572.38 nm and 1.35 pm respectively, which gives a quality factor over 1 million.

wavelength and linewidth of the mode are 1572.38 nm and 1.35 pm, respectively (Fig. 6f), which yields a quality factor of $\sim 1.16 \times 10^6$. While the theoretical quality factor is calculated for a structure free from material loss, in the experiment, material losses induced by two-photon absorption, free-carrier absorption, etc., structure defects induced scattering, and measurement noise will limit the measured quality factor. The quality factor of twisted lattice nanocavities could be further in-

creased by optimizing the fabrication and characterization procedures as well as material systems.

7. Conclusion

We demonstrate a new class of twisted lattice nanocavities based on mode locking in momentum space, which presents a record high

figure of merit of light localization among all reported optical cavities. In stark contrast to the well-studied flatband induced field localization, the twisted lattice nanocavity is free from periodicity requirement, which greatly simplifies fabrication procedure. The quality factor of the nanocavity increases continuously with the decreasing of the twisted angle without fine-tuning any other structure parameters. The highest quality factor obtained by three-dimensional full wave simulation exceeds 200 billion with a mode volume of $\sim 0.048 \lambda^3$. We have further constructed silicon-based twisted lattice nanocavities based on the design. The measured quality factor for the silicon based twisted lattice nanocavities is over 1 million. The demonstrated twisted lattice nanocavities provide a powerful platform to study light-matter interaction for tests of fundamental physics, and promise new functional devices with unprecedented performance from the classical to quantum regime.

Data availability

The authors declare that the main data supporting the findings of this study are available within the article and its Supplementary Information. Extra data are available from the corresponding author upon reasonable request.

Declaration of competing interest

The authors declare that they have no conflicts of interest in this work.

Acknowledgments

This work is supported by the National Key R&D Program of China (2018YFA0704401), the Beijing Natural Science Foundation (Z180011), the National Natural Science Foundation of China (12225402, 91950115, 11774014, 61521004 and 62175003) and the Tencent Foundation.

Supplementary materials

Supplementary material associated with this article can be found, in the online version, at doi:10.1016/j.fmre.2022.11.004.

References

- [1] E. Fermi, Quantum theory of radiation, *Rev. Mod. Phys.* 4 (1932) 87–132.
- [2] E.M. Purcell, Spontaneous emission probabilities at radio frequencies, *Phys. Rev.* 69 (1946) 681.
- [3] K.J. Vahala, Optical microcavities, *Nature* 424 (2003) 839–846.
- [4] M. Ruggenthaler, N. Tancogne-Dejean, J. Flick, et al., From a quantum-electrodynamical light-matter description to novel spectroscopies, *Nat. Rev. Chem.* 2 (2018) 0118.
- [5] A. Frisk Kockum, A. Miranovic, S. De Liberato, et al., Ultrastrong coupling between light and matter, *Nat. Rev. Phys.* 1 (2019) 19–40.
- [6] D.L. Andrews, D.S. Bradshaw, K.A. Forbes, et al., Quantum electrodynamics in modern optics and photonics: tutorial, *J. Opt. Soc. Am. B* 37 (2020) 1153–1172.
- [7] J.D. Joannopoulos, P. Villeneuve, S. Fan, Photonic crystals: putting a new twist on light, *Nature* 386 (1997) 143–149.
- [8] M. Soljačić, J.D. Joannopoulos, Enhancement of nonlinear effects using photonic crystals, *Nat. Mater.* 3 (2004) 211–219.
- [9] S. Noda, M. Fujita, T. Asano, Spontaneous-emission control by photonic crystals and nanocavities, *Nat. Photon.* 1 (2007) 449–458.
- [10] T. Baba, Slow light in photonic crystals, *Nat. Photon.* 2 (2008) 465–473.
- [11] T.J. Kippenberg, K.J. Vahala, Cavity optomechanics: back-action at the mesoscale, *Science* 321 (2008) 1172–1176.
- [12] J.A. Schuller, E.S. Barnard, W.S. Cai, et al., Plasmonics for extreme light concentration and manipulation, *Nat. Mater.* 9 (2010) 193–204.
- [13] D.K. Gramotnev, S.I. Bozhevolnyi, Plasmonics beyond the diffraction limit, *Nat. Photon.* 4 (2010) 83–91.
- [14] Y. Liu, X. Zhang, Metamaterials: a new frontier of science and technology, *Chem. Soc. Rev.* 40 (2011) 2494–2507.
- [15] O. Hess, J.B. Pendry, S.A. Maier, et al., Active nanoplasmonic metamaterials, *Nat. Mater.* 11 (2012) 573–584.
- [16] M. Kauranen, A.V. Zayats, Nonlinear Plasmonics, *Nat. Photon.* 6 (2012) 737–748.
- [17] P. Berini, I. De Leon, Surface plasmon-polariton amplifiers and lasers, *Nat. Photon.* 6 (2012) 16–24.
- [18] M.S. Tame, K.R. McEnery, S.K. Özdemir, et al., Quantum plasmonics, *Nat. Phys.* 9 (2013) 329–340.
- [19] R.M. Ma, R.F. Oulton, Applications of nanolasers, *Nat. Nanotechnol.* 14 (2019) 12–22.
- [20] D.W. Verwooy, V.S. Ilchenko, H. Mabuchi, et al., High-Q measurements of fused-silica microspheres in the near infrared, *Opt. Lett.* 23 (1998) 247–249.
- [21] T.J. Kippenberg, S.M. Spillane, K.J. Vahala, Demonstration of ultra-high-Q small mode volume toroid microcavities on a chip, *Appl. Phys. Lett.* 85 (2004) 6113–6115.
- [22] S.M. Spillane, T.J. Kippenberg, K.J. Vahala, et al., Ultrahigh-Q toroidal microresonators for cavity quantum electrodynamics, *Phys. Rev. A* 71 (2005) 013817.
- [23] P. Del’Haye, A. Schliesser, O. Arcizet, et al., Optical frequency comb generation from a monolithic microresonator, *Nature* 450 (2007) 1214–1217.
- [24] A.A. Savchenkov, A.B. Matsko, V.S. Ilchenko, et al., Optical resonators with ten million finesse, *Opt. Express* 15 (2007) 6768–6773.
- [25] M. Pöllinger, D. O’Shea, F. Warken, et al., Ultrahigh-Q tunable whispering-gallery-mode microresonator, *Phys. Rev. Lett.* 103 (2009) 053901.
- [26] J.G. Zhu, S.K. Özdemir, Y.F. Xiao, et al., On-chip single nanoparticle detection and sizing by mode splitting in an ultrahigh-Q microresonator, *Nat. Photon.* 4 (2010) 46–49.
- [27] X.F. Jiang, L.B. Shao, S.X. Zhang, et al., Chaos-assisted broadband momentum transformation in optical microresonators, *Science* 358 (2017) 344–347.
- [28] A.E. Shitikov, I.A. Bilenko, N.M. Kondratiev, et al., Billion Q-factor in silicon WGM resonators, *Optica* 5 (2018) 1525–1528.
- [29] B.-S. Song, S. Noda, T. Asano, et al., Ultra-high-Q photonic double-heterostructure nanocavity, *Nat. Mater.* 4 (2005) 207–210.
- [30] Q.M. Quan, M. Loncar, Deterministic design of wavelength scale, ultra-high Q photonic crystal nanobeam cavities, *Opt. Express* 19 (2011) 18529–18542.
- [31] Y. Lai, S. Pirotta, G. Urbinati, et al., Genetically designed L3 photonic crystal nanocavities with measured quality factor exceeding one million, *Appl. Phys. Lett.* 104 (2014) 241101.
- [32] F. Alpeggiani, L.C. Andreani, D. Gerace, Effective bichromatic potential for ultra-high Q-factor photonic crystal slab cavities, *Appl. Phys. Lett.* 107 (2015) 261110.
- [33] M. Minkov, V. Savona, D. Gerace, Photonic crystal slab cavity simultaneously optimized for ultra-high Q/V and vertical radiation coupling, *Appl. Phys. Lett.* 111 (2017) 131104.
- [34] T. Asano, Y. Ochi, Y. Takahashi, et al., Photonic crystal nanocavity with a Q factor exceeding eleven million, *Opt. Express* 25 (2017) 1769–1777.
- [35] H. Choi, M. Heuck, D. Englund, Self-similar nanocavity design with ultrasmall mode volume for single-photon nonlinearities, *Phys. Rev. Lett.* 118 (2017) 223605.
- [36] T. Asano, S. Noda, Optimization of photonic crystal nanocavities based on deep learning, *Opt. Express* 26 (2018) 32704–32717.
- [37] M.X. Li, H.X. Liang, R. Luo, et al., Photon-level tuning of photonic nanocavities, *Optica* 6 (2019) 860–863.
- [38] B.-S. Song, T. Asano, S. Jeon, et al., Ultrahigh-Q photonic crystal nanocavities based on 4H silicon carbide, *Optica* 6 (2019) 991–995.
- [39] J. Kern, S. Großmann, N.V. Tarakina, et al., Atomic-scale confinement of resonant optical fields, *Nano Lett.* 12 (2012) 5504–5509.
- [40] C. Ciraci, R.T. Hill, J.J. Mock, et al., Probing the ultimate limits of plasmonic enhancement, *Science* 337 (2012) 1072–1074.
- [41] R. Chikkaraddy, B. De Nijs, F. Benz, et al., Single-molecule strong coupling at room temperature in plasmonic nanocavities, *Nature* 535 (2016) 127–130.
- [42] J.J. Baumberg, J. Aizpurua, M.H. Mikkelsen, et al., Extreme nanophotonics from ultrathin metallic gaps, *Nat. Mater.* 18 (2019) 668–678.
- [43] I. Epstein, D. Alcaraz, Z.Q. Huang, et al., Far-field excitation of single graphene plasmon cavities with ultracompressed mode volumes, *Science* 368 (2020) 1219–1223.
- [44] W.C. Li, Q. Zhou, P. Zhang, et al., Bright optical eigenmode of 1 nm^3 mode volume, *Phys. Rev. Lett.* 126 (2021) 257401.
- [45] Z.J. Liu, Y. Xu, Y. Lin, et al., High-Q quasibound states in the continuum for nonlinear metasurfaces, *Phys. Rev. Lett.* 123 (2019) 253901.
- [46] K. Koshelev, S. Kruk, E. Melik-Gaykazyan, et al., Subwavelength dielectric resonators for nonlinear nanophotonics, *Science* 367 (2020) 288–292.
- [47] Z.J. Liu, J.Y. Wang, B. Chen, et al., Giant enhancement of continuous wave second harmonic generation from few-layer GaSe coupled to high-Q quasi bound states in the continuum, *Nano Lett.* 21 (2021) 7405–7410.
- [48] Y. Yu, A. Sakanas, A.R. Zali, et al., Ultra-coherent Fano laser based on a bound state in the continuum, *Nat. Photon.* 15 (2021) 758–764.
- [49] Z.H. Chen, X.F. Yin, J.C. Jin, et al., Observation of miniaturized bound states in the continuum with ultra-high quality factors, *Sci. Bull.* 67 (2022) 359–366.
- [50] Y. Cao, V. Fatemi, A. Demir, et al., Correlated insulator behaviour at half-filling in magic-angle graphene superlattices, *Nature* 556 (2018) 80–84.
- [51] Y. Cao, V. Fatemi, S.A. Fang, et al., Unconventional superconductivity in magic-angle graphene superlattices, *Nature* 556 (2018) 43–50.
- [52] D. Huang, J. Choi, C.-K. Shih, et al., Excitons in semiconductor moiré superlattices, *Nat. Nanotechnol.* 17 (2022) 227–238.
- [53] S.S. Sunku, G.X. Ni, B.Y. Jiang, et al., Photonic crystals for nano-light in moiré graphene superlattices, *Science* 362 (2018) 1153–1156.
- [54] P. Wang, Y.L. Zheng, X.F. Chen, et al., Localization and delocalization of light in photonic moiré lattices, *Nature* 577 (2020) 42–46.
- [55] X.R. Mao, Z.K. Shao, H.Y. Luan, et al., Magic-angle lasers in nanostructured moiré superlattice, *Nat. Nanotechnol.* 16 (2021) 1099–1105.

- [56] M. Oudich, G.X. Su, Y.C. Deng, et al., Photonic analog of bilayer graphene, *Phys. Rev. B* 103 (2021) 214311.
- [57] K.C. Dong, T.C. Zhang, J.C. Li, et al., Flat bands in magic-angle bilayer photonic crystals at small twists, *Phys. Rev. Lett.* 126 (2021) 223601.
- [58] J.L. Chen, X. Lin, M.Y. Chen, et al., A perspective of twisted photonic structures, *Appl. Phys. Lett.* 119 (2021) 240501.
- [59] Z.B. Zheng, F.S. Sun, W.C. Huang, et al., Phonon polaritons in twisted double-layers of hyperbolic van der Waals crystals, *Nano Lett.* 20 (2020) 5301–5308.
- [60] G.W. Hu, Q.D. Ou, G.Y. Si, et al., Topological polaritons and photonic magic angles in twisted α -MoO₃ bilayers, *Nature* 582 (2020) 209–213.
- [61] J.H. Duan, N. Capote-Robayna, J. Taboada-Gutiérrez, et al., Twisted nano-optics: manipulating light at the nanoscale with twisted phonon polaritonic slabs, *Nano Lett.* 20 (2020) 5323–5329.
- [62] M.Y. Chen, X. Lin, T.H. Dinh, et al., Configurable phonon polaritons in twisted α -MoO₃, *Nat. Mater.* 19 (2020) 1307–1311.
- [63] Y.C. Deng, M. Oudich, N.JRK Gerard, et al., Magic-angle bilayer phononic graphene, *Phys. Rev. B* 102 (2020) 180304.
- [64] M.R. López, F. Peñaranda, J. Christensen, et al., Flat bands in magic-angle vibrating plates, *Phys. Rev. Lett.* 125 (2020) 214301.



Ren-Min Ma is a professor of physics at Peking University. Dr. Ma received his PhD degree in physics from Peking University in 2009. He was a postdoc researcher at UC Berkeley during 2009 to 2014 before joining Peking University as a faculty. His research interests include laser physics, nanophotonics, non-Hermitian and topological photonics. His works has been selected as China's Top 10 Optical Breakthroughs of 2018 and 2020, APS Physics "Highlights of the Year" 2018, China's Top 10 Semiconductor Research Breakthroughs 2020. In 2021, he received Xplorer Prize, and Early-Career Award in Nanophotonics. In 2022, he received China National Funds for Distinguished Young Scientists.